ARCHIVES OF ELECTRICAL ENGINEERING VOL. X(Y), pp. 1-25 (2026)

This paper has been accepted for publication in the AEE journal. This is the version, which has not been fully edited and content may change prior to final publication.
Citation information: DOI 10.24425/aee.2026.158258

Laplace-based solution for three-phase short-circuit fault in synchronous machines

GERMÁN GUEVARA*, **DANILO RAIRÁN**

Technological Faculty, Francisco José de Caldas District University
13th Street # 31–75, 111611537 Bogotá, Colombia
*e-mail: {*gaguevarav/drairan}@udistrital.edu.co*

Abstract: The study of synchronous machine behavior under transient conditions caused by a three-phase short-circuit fault is primarily based on two approaches: experimental analysis and simulation. Experimentally, the sudden three-phase short-circuit test applied to the machine yields a low-parameter empirical 'short-circuit function' that models it in a simple manner using the equivalent 'constant voltage behind reactance' circuit. On the other hand, fault analysis is performed through simulation using Electromagnetic Transient Programs, which are based on numerical discretization methods. However, in both cases, there is a lack of formal analytical descriptions of a generator's transient behavior. In contrast, this paper introduces a closed-form solution using Laplace, as an alternative method for computing three-phase short-circuit faults. This deterministic approach provides an analytical description of the machine represented by different model structures, facilitates the study of transient interactions among its windings, and enables the analysis of current components (synchronous, dc, and double frequency). Additionally, the closed-form solution is compared with a numerical integration method in terms of computational efficiency, processing time, and accuracy. This demonstrates the existence of a closed-form solution for the generator in the transient state and highlights its advantages for modeling and computation compared with current methods.
Key words: generator, power system, synchronous machine, three-phase fault current, three-phase short-circuit

1. Introduction

The formal analytical description of the transient behavior of the Synchronous Machine (SM) is limited due to the current calculation methods available for solving such transients when the machine encounters a three-phase short-circuit condition. This description primarily involves observing short-circuit current curves over time, obtained by numerically integrating the SM model structure in the phase domain using a diversity of Electromagnetic Transient Programs (EMTPs) [1–10, 17]. Additionally, an empirical "short-circuit function" is employed [11] (p. 234, Eq. (F.5)), characterized by a model structure (constant voltage behind reactance) that highlights the simplicity of the current SM description. This function is a minimally

This paper has been accepted for publication in the AEE journal. This is the version, which has not been fully edited and content may change prior to final publication.
Citation information: DOI 10.24425/aee.2026.158258

parameterized equation, focusing solely on direct-axis components, mainly estimated from Sudden Short-Circuit (SSC) tests [11] (pp. 136–140).

This paper presents the deterministic mathematical solution for the three-phase short-circuit generator, represented by its model structure in the "*dq domain*," which is then transformed into the time domain using the inverse Park transformation. This closed-form solution provides the formal analytical description of the SM in transient state, as shown below.

The solved model structure enables the characterization of windings using equivalent circuits with lumped parameters along the *d* and *q*-axes and may include a variable number of damper windings in the rotor varying models' complexity [12] (pp. 6–15). Reference [12] (pp. 30–55) summarizes the techniques used to derive model structure parameters based on measurements performed on the machine. Among the most relevant tests for parameter determination are the three-phase, no-load, sudden-short-circuit test, the load rejection test, and the Standstill Frequency Response (SSFR) test. The SSFR test [11] (pp. 179–211) is applicable to large salient-pole generators [13].

The modeling of the SM for transient-state analysis [14–17] leads to its general voltage equation in the 0*dq* domain, which in this study is shown to be consistent with the chosen model structure for analysis. The machine's voltage Ordinary Differential Equation (ODE) is then applied to the three-phase short-circuit condition and, as a novel contribution, solved using Laplace (the basic solution algorithm is presented). The solution yields a "short-circuit function," providing a closed-form solution to the SM model under three-phase short-circuit conditions.

In this paper we show how the analytical expression of the short-circuit function obtained from the closed-form solution, independent of the complexity of the SM model (the results are presented for model structures 1.0, 2.0, and 2.1.), describes all the transients, which are simultaneous and interrelated among windings. The closed-form solution reveals that the angular frequency of the SM changes from steady-state to transient and enables evaluation of the reasons behind this change.

The short-circuit function obtained also enables the identification of the classical components observed in the SSC test, namely, the *fundamental frequency component* or *ac*, *the dc component*, and *the second harmonic component* (double frequency). These three components are not only analytically described for each phase of the SM armature but consider the impact of the δ angle in the description.

The closed-form solution enables a detailed analytical understanding of "*the impact of each winding*" on the three-phase fault current, defining its behavior across time intervals determined by the short-circuit constants derived from this deterministic calculation.

Finally, this paper evaluates the significant advantage that the closed-form solution offers over a current numerical integration simulation method in terms of the elapsed time, computational effort, and result accuracy.

This paper has been accepted for publication in the AEE journal. This is the version, which has not been fully edited and content may change prior to final publication.
Citation information: DOI 10.24425/aee.2026.158258

2. Synchronous machine model in the *dq* domain

Figure 1 illustrates the SM with three armature windings corresponding to phases *a*, *b* and *c*, the field winding *F* and the damping windings *D* and *Q* [14, 17]. It is shown there the *d*-axis ahead of the magnetic axis of phase *a* (reference axis) by the angle θ, to represent this, the *q*-axis must be considered shifted from the reference axis at an angle δ, depending on the load of the SM, thus:

$$\theta = \omega_s\, t + 90° + \delta. \tag{1}$$

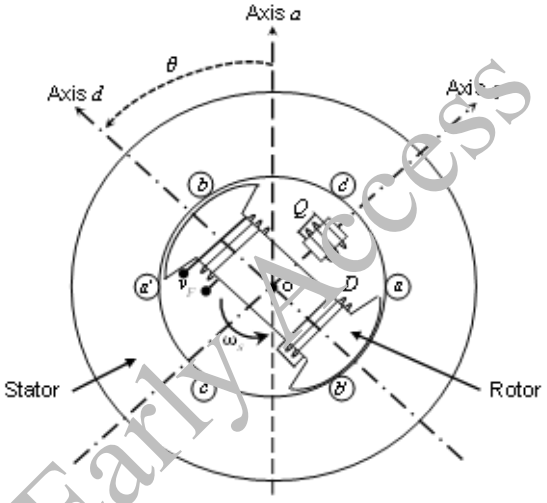

Fig. 1. Representation of the windings in the synchronous machine

Table 1 records the hypothetical parameter values (inductances adjusted for saturation [18−20]), assumed to have been estimated from SSFR test data obtained from a 285 MVA, 30 kV, 60 Hz synchronous machine, with a field voltage of 300 V; this machine will be used as an example in this paper.

Table 1. Generator parameters with the model structure in Fig. 2

Self-inductances	**Mutual inductances**	**Resistances**
L_d = 4.5 mH	M_r = 75 mH	R_a = 2.5 mΩ
L_q = 4.2 mH	M_F = 60 mH	R_F = 0.5 Ω
L_F = 1.5 H	M_D = 3.2 mH	R_D = 12 mΩ
L_D = 4.0 mH	M_Q = 1.6 mH	R_Q = 12 mΩ

This paper has been accepted for publication in the AEE journal. This is the version, which has not been fully edited and content may change prior to final publication.
Citation information: DOI 10.24425/aee.2026.158258

L_Q = 1.0 mH		

The objective of the research is to present a closed-form solution of the generator subjected to a three-phase short-circuit fault; therefore, it is sufficient to rely on the original Park theory [21, 22], in which harmonic distortion can be neglected during this transient state of the machine because the fault is symmetrical.

Based on Park's work, the variables in the *abc* axes are related to the variables in the 0*dq* axes through the normalized matrix $\boldsymbol{P}$, given by:

$$\boldsymbol{P} = \sqrt{2/3}\begin{pmatrix} \frac{1}{\sqrt{2}} & \frac{1}{\sqrt{2}} & \frac{1}{\sqrt{2}} \\ \cos\theta & \cos(\theta - 120°) & \cos(\theta + 120°) \\ \sin\theta & \sin(\theta - 120°) & \sin(\theta + 120°) \end{pmatrix}. \tag{2}$$

The Park transformation matrix is orthogonal, meaning $\boldsymbol{P}^{-1} = \boldsymbol{P}^{T}$, ensuring power invariance through the transformation, thus:

$$\boldsymbol{P}^{-1} = \sqrt{2/3}\begin{pmatrix} \frac{1}{\sqrt{2}} & \cos\theta & \sin\theta \\ \frac{1}{\sqrt{2}} & \cos(\theta - 120°) & \sin(\theta - 120°) \\ \frac{1}{\sqrt{2}} & \cos(\theta + 120°) & \sin(\theta + 120°) \end{pmatrix} = \boldsymbol{P}^{T}. \tag{3}$$

The angle θ represents the steady-state phase shift (assuming constant ω), occurring between the two axis systems at the time of transformation. According to (1), if the axis transformation occurs at $t = 0$, then the phase difference between the two systems is $\theta = \delta_0$, and *the flux linkages are functions of the machine's power angle.*

The Park transformation for the machine's fluxes, voltages, and currents is as follows:

$$\boldsymbol{\psi}_{0dq} = \boldsymbol{P}\boldsymbol{\psi}_{abc}, \quad \boldsymbol{V}_{0dq} = \boldsymbol{P}\boldsymbol{V}_{abc}, \quad \boldsymbol{I}_{0dq} = \boldsymbol{P}\boldsymbol{I}_{abc}. \tag{4}$$

From Eq. (4), it is also deduced that:

$$\boldsymbol{\psi}_{abc} = \boldsymbol{P}^{-1}\boldsymbol{\psi}_{0dq}, \quad \boldsymbol{V}_{abc} = \boldsymbol{P}^{-1}\boldsymbol{V}_{0dq}, \quad \boldsymbol{I}_{abc} = \boldsymbol{P}^{-1}\boldsymbol{I}_{0dq}. \tag{5}$$

The *general equation for the voltage* of the synchronous machine in the *abc* system is written in compact form as:

$$\begin{pmatrix} \boldsymbol{V}_{abc} \\ \boldsymbol{V}_{FDQ} \end{pmatrix} = -\begin{pmatrix} \boldsymbol{R}_{ss} & 0 \\ 0 & \boldsymbol{R}_{rr} \end{pmatrix}\begin{pmatrix} \boldsymbol{I}_{abc} \\ \boldsymbol{I}_{FDQ} \end{pmatrix} - \frac{\mathrm{d}}{\mathrm{d}t}\begin{pmatrix} \boldsymbol{\psi}_{abc} \\ \boldsymbol{\psi}_{FDQ} \end{pmatrix}, \tag{6}$$

where the flux linkage vector is given by:

$$\begin{pmatrix} \boldsymbol{\psi}_{abc} \\ \boldsymbol{\psi}_{FDQ} \end{pmatrix} = \begin{pmatrix} \boldsymbol{L}_{ss} & \boldsymbol{L}_{sr} \\ \boldsymbol{L}_{rs} & \boldsymbol{L}_{rr} \end{pmatrix}\begin{pmatrix} \boldsymbol{I}_{abc} \\ \boldsymbol{I}_{FDQ} \end{pmatrix}. \tag{7}$$

The vectors $\boldsymbol{\psi}_{abc}$ and $\boldsymbol{\psi}_{FDQ}$ have elements representing the instantaneous values of flux linkages of the corresponding windings $\boldsymbol{I}_{abc}$ and $\boldsymbol{I}_{FDQ}$ are the instantaneous values of current for

This paper has been accepted for publication in the AEE journal. This is the version, which has not been fully edited and content may change prior to final publication.
Citation information: DOI 10.24425/aee.2026.158258

the corresponding windings; and the subscripts *s* and *r* in the inductances $\boldsymbol{L}$ designate these parameters as referring to the stator and the rotor, respectively. Thus, the submatrix $\boldsymbol{L}_{ss}$ contains the elements of the stator inductances; the submatrix $\boldsymbol{L}_{sr}$ contains the mutual inductances between the stator and the rotor (where $\boldsymbol{L}_{sr} = \boldsymbol{L}_{rs}^{T}$); and the submatrix $\boldsymbol{L}_{rr}$ consists of the rotor inductances. So, the expressions for the self and mutual inductances of the elements of the submatrix $\boldsymbol{L}_{ss}$, for the salient-pole generator, are:

$$\boldsymbol{L}_{ss} = \begin{pmatrix} L_s + L_m \cos 2\,\theta & -M_s + L_m \cos 2\,(\theta - 120°) & -M_s + L_m \cos 2\,(\theta + 120°) \\ -M_s + L_m \cos 2\,(\theta - 120°) & L_s + L_m \cos 2\,(\theta - 120°) & -M_s + L_m \cos 2\,\theta \\ -M_s + L_m \cos 2\,(\theta + 120°) & -M_s + L_m \cos 2\,\theta & L_s + L_m \cos 2\,(\theta + 120°) \end{pmatrix}. \quad (8)$$

L_s is the constant part of the L_a and independent of the rotor angle θ, while L_m is the coefficient of the variable part of L_a, depending on θ, and consequently time. For phases *b* and *c*, the corresponding self-inductance is obtained considering the 120° phase difference between these windings and with respect to phase *a*. M_s is the constant part of L_{ba} and independent of the rotor angle θ. Considering the 120° phase difference, expressions for the mutual inductances L_{ca} and L_{bc}; additionally, $L_{ab} = L_{ba}$; $L_{bc} = L_{cb}$; $L_{ac} = L_{ca}$.

The order of the $\boldsymbol{L}_{sr}$ and $\boldsymbol{L}_{ss}$ submatrices depends on the level of complexity used to represent the SM. From Table 1 in [12], model 2.1 (considered the best fit for the SM shown in Figure 1) and model 1.0 are selected. The voltage equation of the SM with the 2.0 model structure is also presented; although it is not considered in [12], it is of interest in [11].

2.1. Model structure 2.1

Model structure 2.1, in Fig. 2, is represented in the form of mutually coupled equivalent circuits.

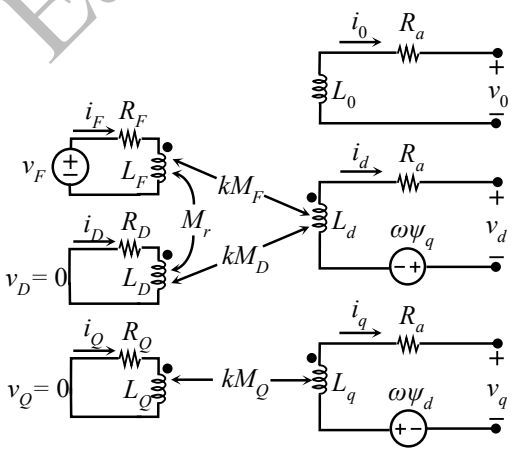

Fig. 2. Equivalent circuits for the model structure 2.1 of the SM in the 0*dq* domain

This paper has been accepted for publication in the AEE journal. This is the version, which has not been fully edited and content may change prior to final publication.
Citation information: DOI 10.24425/aee.2026.158258

Figure 2 shows that in the rotor of the SM there are two windings on the *d*-axis and one on the *q*-axis, hence the numbering 2.1 for its model structure. Thus, the SM is represented using the damping winding in the *abc* system, as shown in Fig. 1, which is fully modeled in both axes of the 0*dq* system.

The elements of the submatrix $\boldsymbol{L}_{sr}$ indicated in (7) for model structure 2.1 are shown in Eq. (9).

$$\boldsymbol{L}_{sr} = \begin{pmatrix} M_F \cos\theta & M_D \cos\theta & M_Q \sin\theta \\ M_F \cos(\theta - 120°) & M_D \cos(\theta - 120°) & M_Q \sin(\theta - 120°) \\ M_F \cos(\theta + 120°) & M_D \cos(\theta + 120°) & M_Q \sin(\theta + 120°) \end{pmatrix} = \boldsymbol{L}_{rs}^T. \tag{9}$$

The elements of the submatrix $\boldsymbol{L}_{rr}$ are constant. There is no magnetic coupling between any of the two windings whose magnetic axis is in the *d*-axis (windings *F* and *D*) and the quadrature-axis damping winding *q*, due to the 90° angular difference between these two axes. Therefore, $L_{FQ} = L_{QF} = L_{DQ} = L_{QD} = 0$. Thus, $\boldsymbol{L}_{rr}$ is given by:

$$\boldsymbol{L}_{rr} = \begin{pmatrix} L_F & M_r & 0 \\ M_r & L_D & 0 \\ 0 & 0 & L_Q \end{pmatrix}. \tag{10}$$

Equation (7), for the flux linkages of the SM referred to the 0*dq* axes, is obtained by replacing Eq. (5) inside it for flux and current, without affecting the original expressions of the rotor flux linkages $\boldsymbol{\psi}_{FDQ}$. Then, we operate $\boldsymbol{P}$ and $\boldsymbol{P}^{-1}$ defined in (2) and (3), respectively, with the submatrices of inductances given by Eq. (8), (9), and (10), noting that $\boldsymbol{L}_{rs}\boldsymbol{P}^{-1} = \boldsymbol{L}_{rs}\boldsymbol{P}^T = (\boldsymbol{P}\boldsymbol{L}_{sr})^T$. In this way, Eq. (7) can be expressed as:

$$\begin{pmatrix} \psi_0 \\ \psi_d \\ \psi_q \\ \psi_F \\ \psi_D \\ \psi_Q \end{pmatrix} = \begin{pmatrix} L_0 & 0 & 0 & 0 & 0 & 0 \\ 0 & L_d & 0 & kM_F & kM_D & 0 \\ 0 & 0 & L_q & 0 & 0 & kM_Q \\ 0 & kM_F & 0 & L_F & M_r & 0 \\ 0 & kM_D & 0 & M_r & L_D & 0 \\ 0 & 0 & kM_Q & 0 & 0 & L_Q \end{pmatrix}, \tag{11}$$

where $k = \sqrt{1.5}$ and the elements L_0, L_d and L_q are related to (8) through:

$$\begin{aligned} L_0 &= L_s - 2M_s, \\ L_d &= L_s + M_s + 1.5L_m, \\ L_q &= L_s + M_s - 1.5L_m. \end{aligned} \tag{12}$$

From Eq. (12), it can be seen that $L_s = \frac{1}{3}\left(L_0 + L_d + L_q\right)$ and $L_m = \frac{1}{3}\left(L_d - L_q\right)$.

By replacing Eq. (5) for voltages and currents in (6), while keeping in mind the flux linkage matrix obtained in (11) and substituting Eq. (5) for voltages and currents in (6), we obtain *the general voltage equation* (13) of the SM in the 0*dq* domain, corresponding to its model structure 2.1.

This paper has been accepted for publication in the AEE journal. This is the version, which has not been fully edited and content may change prior to final publication.
Citation information: DOI 10.24425/aee.2026.158258

$$\boldsymbol{V}_{(2.1)} = -\boldsymbol{R}_{(2.1)}\boldsymbol{I}_{(2.1)} - \boldsymbol{L}_{(2.1)}\frac{\mathrm{d}}{\mathrm{d}t}\boldsymbol{I}_{(2.1)}, \tag{13}$$

where:

$$\boldsymbol{V}_{(2.1)} = \begin{pmatrix} v_0 \\ v_d \\ v_q \\ -v_F \\ 0 \\ 0 \end{pmatrix}, \qquad \boldsymbol{I}_{(2.1)} = \begin{pmatrix} i_0 \\ i_d \\ i_q \\ i_F \\ i_D \\ i_Q \end{pmatrix}, \tag{14}$$

$$\boldsymbol{R}_{(2.1)} = \begin{pmatrix} R_a & 0 & 0 & 0 & 0 & 0 \\ 0 & R_a & \omega L_q & 0 & 0 & k\omega M_Q \\ 0 & -\omega L_d & R_a & -k\omega M_F & -k\omega M_D & 0 \\ 0 & 0 & 0 & R_F & 0 & 0 \\ 0 & 0 & 0 & 0 & R_D & 0 \\ 0 & 0 & 0 & 0 & 0 & R_Q \end{pmatrix}, \tag{15}$$

$$\boldsymbol{L}_{(2.1)} = \begin{pmatrix} L_0 & 0 & 0 & 0 & 0 & 0 \\ 0 & L_d & 0 & kM_F & kM_D & 0 \\ 0 & 0 & L_q & 0 & 0 & kM_Q \\ 0 & kM_F & 0 & L_F & M_r & 0 \\ 0 & kM_D & 0 & M_r & L_D & 0 \\ 0 & 0 & kM_Q & 0 & 0 & L_Q \end{pmatrix}. \tag{16}$$

2.2. Model structure 2.0

Model structure 2.0, in Fig. 3, is represented in the form of mutually coupled equivalent circuits.

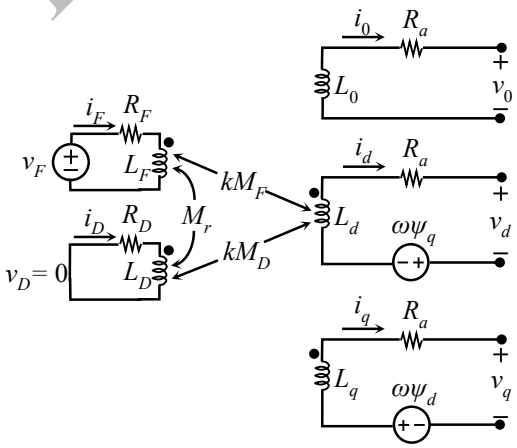

Fig. 3. Equivalent circuits for the model structure 2.0 of the SM in the 0dq domain

This paper has been accepted for publication in the AEE journal. This is the version, which has not been fully edited and content may change prior to final publication.
Citation information: DOI 10.24425/aee.2026.158258

Figure 3 shows that in the rotor of the SM for its model structure 2.0 there are two windings on the *d*-axis and none on the *q*-axis. Thus, the damping winding of the SM in the *abc* system is modeled only on the *d*-axis of the 0*dq* system. The expressions of the elements of the submatrix $\boldsymbol{L}_{sr}$ in Eq. (7) in the *abc* system for model structure 2.0 are all functions of time and applicable to both types of synchronous generators (salient or cylindrical poles; in the cylindrical rotor type, winding *D* represents the parasitic currents in this part of the machine); then:

$$\boldsymbol{L}_{sr} = \begin{pmatrix} M_F \cos\theta & M_D \cos\theta \\ M_F \cos(\theta - 120°) & M_D \cos(\theta - 120°) \\ M_F \cos(\theta + 120°) & M_D \cos(\theta + 120°) \end{pmatrix} = \boldsymbol{L}_{rs}^{T}. \tag{17}$$

In both types of generators, the magnetic fluxes of the rotor windings do not depend on the rotor position; therefore, the elements of the submatrix $\boldsymbol{L}_{rr}$ are constant amounts. There is magnetic coupling between the field winding *F* and the winding *D* since they share the same *d*-axis, hence, $L_{FD} = L_{DF} = M_r$. Thus, $\boldsymbol{L}_{rr}$ is given by:

$$\boldsymbol{L}_{rr} = \begin{pmatrix} L_F & M_r \\ M_r & L_D \end{pmatrix}. \tag{18}$$

The *general voltage equation* (19) of the SM corresponding to its model structure 2.0 is obtained using a similar procedure as described to determine the matrix equation of model 2.1.

$$\boldsymbol{V}_{(2.0)} = -\boldsymbol{R}_{(2.0)}\boldsymbol{I}_{(2.0)} - \boldsymbol{L}_{(2.0)}\frac{\mathrm{d}}{\mathrm{d}t}\boldsymbol{I}_{(2.0)}, \tag{19}$$

where:

$$\boldsymbol{V}_{(2.0)} = \begin{pmatrix} v_0 \\ v_d \\ v_q \\ -v_F \\ 0 \end{pmatrix}, \qquad \boldsymbol{I}_{(2.0)} = \begin{pmatrix} i_0 \\ i_d \\ i_q \\ i_F \\ i_D \end{pmatrix}, \tag{20}$$

$$\boldsymbol{R}_{(2.0)} = \begin{pmatrix} R_a & 0 & 0 & 0 & 0 \\ 0 & R_a & \omega L_q & 0 & 0 \\ 0 & -\omega L_d & R_a & -k\omega M_F & -k\omega M_D \\ 0 & 0 & 0 & R_F & 0 \\ 0 & 0 & 0 & 0 & R_D \end{pmatrix}, \tag{21}$$

$$\boldsymbol{L}_{(2.0)} = \begin{pmatrix} L_0 & 0 & 0 & 0 & 0 \\ 0 & L_d & 0 & kM_F & kM_D \\ 0 & 0 & L_q & 0 & 0 \\ 0 & kM_F & 0 & L_F & M_r \\ 0 & kM_D & 0 & M_r & L_D \end{pmatrix}. \tag{22}$$

This paper has been accepted for publication in the AEE journal. This is the version, which has not been fully edited and content may change prior to final publication.
Citation information: DOI 10.24425/aee.2026.158258

2.3. Model structure 1.0

Model structure 1.0 is represented in the form of mutually coupled equivalent circuits as shown in Fig. 4.

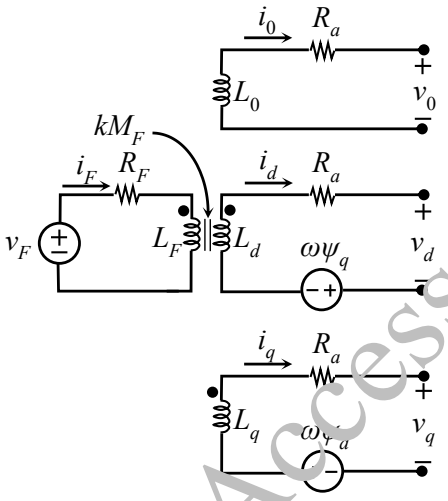

Fig. 4. Equivalent circuits for the model structure 1.0 of the SM in the 0*dq* domain

Figure 4 shows that there is one winding on the *d*-axis and none on the *q*-axis in the rotor of the SM for the model structure 1.0. Thus, the SM in the *abc* system is modeled without the damping winding. For this case, the submatrices $\boldsymbol{L}_{sr}$ and $\boldsymbol{L}_{rr}$ of (7) for the SM in the *abc* system are given by Eqs. (23) and (24), respectively.

$$\boldsymbol{L}_{sr} = \begin{pmatrix} M_F \cos\theta \\ M_F \cos(\theta - 120°) \\ M_F \cos(\theta + 120°) \end{pmatrix} = \boldsymbol{L}_{rs}^{T}, \tag{23}$$

$$\boldsymbol{L}_{rr} = L_F. \tag{24}$$

Thus, the *general voltage equation* (6) of the SM corresponding to model structure 1.0 is shown in (25).

$$\boldsymbol{V}_{(2.0)} = -\boldsymbol{R}_{(2.0)}\boldsymbol{I}_{(2.0)} - \boldsymbol{L}_{(2.0)}\frac{\mathrm{d}}{\mathrm{d}t}\boldsymbol{I}_{(2.0)}, \tag{25}$$

where:

$$\boldsymbol{V}_{(1.0)} = \begin{pmatrix} v_0 \\ v_d \\ v_q \\ -v_F \end{pmatrix}, \qquad \boldsymbol{I}_{(1.0)} = \begin{pmatrix} i_0 \\ i_d \\ i_q \\ i_F \end{pmatrix}, \tag{26}$$

This paper has been accepted for publication in the AEE journal. This is the version, which has not been fully edited and content may change prior to final publication.
Citation information: DOI 10.24425/aee.2026.158258

$$\boldsymbol{R}_{(1.0)} = \begin{pmatrix} R_a & 0 & 0 & 0 \\ 0 & R_a & \omega L_q & 0 \\ 0 & -\omega L_d & R_a & -k\omega M_F \\ 0 & 0 & 0 & R_F \end{pmatrix}, \tag{27}$$

$$\boldsymbol{L}_{(1.0)} = \begin{pmatrix} L_0 & 0 & 0 & 0 \\ 0 & L_d & 0 & kM_F \\ 0 & 0 & L_q & 0 \\ 0 & kM_F & 0 & L_F \end{pmatrix}. \tag{28}$$

Equations (13), (19) and (25) are expressed as follows:

$$\boldsymbol{V} = -\boldsymbol{R}\boldsymbol{I} - \boldsymbol{L}\frac{\mathrm{d}}{\mathrm{d}t}\boldsymbol{I}. \tag{29}$$

In (29), the expression for voltage is a linear differential equation with constant coefficients (assuming constant ω).

3. Closed-form solution of the synchronous machine during short-circuit fault

The model structure in the 0*dq* domain given by (29) has a known deterministic solution. Thomas A. Lipo uses eigenvalue-eigenvector techniques, known as "modal theory," to solve the transient condition of the SM due to a three-phase fault [23]. In contrast, Gibson H.M. Sianipar presents a solution procedure [24] that departs from the model in (29) and uses the eigenvalues of the state-space system matrix [25, 26]. Although Sianipar presents an equation for the current in the *dq* system in terms of summations, there is no evidence of an explicit example in his paper. Unlike the calculation approaches mentioned, this paper presents the closed-form solution of the three-phase short-circuit current vector shown in (29) using Laplace Transformation.

Armature and field winding currents for the generator described in Table 1 will be analytically determined under no-load, constant speed, and excitation conditions, in the event of a three-phase to earth short-circuit fault (it is possible to consider the fault through an impedance to ground).

The terminal voltage of the SM operating in steady state is given by:

$$\begin{pmatrix} v_a \\ v_b \\ v_c \end{pmatrix} = \begin{pmatrix} \sqrt{2}V\cos(\omega_s t + \theta_{a-dq}) \\ \sqrt{2}V\cos(\omega_s t - 120° + \theta_{a-dq}) \\ \sqrt{2}V\cos(\omega_s t + 120° + \theta_{a-dq}) \end{pmatrix}. \tag{30}$$

The angle $\theta_{a\text{-}dq}$ in Eq. (30) is 0° or –90° depending on the alignment between the magnetic axis of phase *a*, and the magnetic *d*-axis or *q*-axis, respectively. Thus, and due to the balanced condition $v_a + v_b + v_c = 0$ and the equation for voltages in Eq. (4), the constant vector $\boldsymbol{V}_{0dq}$ is given in Table 2.

This paper has been accepted for publication in the AEE journal. This is the version, which has not been fully edited and content may change prior to final publication.
Citation information: DOI 10.24425/aee.2026.158258

During the three-phase fault, phase voltages are $v_a = v_b = v_c = 0$, hence $v_0 = v_d = v_q = 0$.

Table 2. Vector $\boldsymbol{V}_{0dq}$ according to magnetic axis alignment

$\boldsymbol{V_{0dq}}$	$\boldsymbol{\theta_{a\text{-}d} = 0°}$	$\boldsymbol{\theta_{a\text{-}q} = -90°}$
v_0	0	0
v_d	$\sqrt{3}V$	0
v_q	0	$\sqrt{3}V$

From Eq. (4) for currents, the vector $\boldsymbol{I}_{0dq}$ is given by:

$$\begin{aligned} i_0 &= \tfrac{1}{\sqrt{3}}(i_a + i_b + i_c), \\ i_d &= \sqrt{2/3}\,(-\sin(\omega t)i_a + \sin(\omega t + 60°)i_b - \cos(\omega t + 30°)i_c), \\ i_q &= \sqrt{2/3}\,(\cos(\omega t)i_a - \cos(\omega t + 60°)i_b - \sin(\omega t + 30°)i_c). \end{aligned} \tag{31}$$

In (31), $i_a + i_b + i_c = 0$ because the fault is balanced, hence $i_0 = 0$, which agrees with the result for v_0, thus, the zero-sequence equation in (29) is not considered. Since the generator is unloaded, $i_a(0) = i_b(0) = i_c(0) = 0$, so in (31), $i_d(0) = i_q(0) = 0$. The initial field current is determined from $i_F(0) = v_F/r_F$.

The closed-form solution for the three-phase short-circuit currents i_d and i_q in (31), along with the currents i_F, i_D, and i_Q, is obtained by applying the Laplace transformation to Eq. (29), as outlined in Eq. (32), as shown in Algorithm 1.

$$\frac{\mathrm{d}}{\mathrm{d}t}\boldsymbol{I} + \boldsymbol{L}^{-1}\boldsymbol{R}\boldsymbol{I} = -\boldsymbol{L}^{-1}\boldsymbol{V}. \tag{32}$$

Algorithm 1. Data: Define the model, $\boldsymbol{L}$, $\boldsymbol{R}$, V_F.

1. Calculate $i_F 0$ from V_F and R_F
2. Define vectors and matrix according to the Model
3. Define $\boldsymbol{V}$, $\boldsymbol{I}$, vectors, see eqs. (14), (20), (26)
4. Define system matrix $\boldsymbol{A}$, from eq. (32)
5. Convert $\boldsymbol{A}$ to *vpa*
6. Define constants vector $\boldsymbol{B}$, Laplace to eq. (32)
7. D ← Compute determinant of $\boldsymbol{A}$
8. **for** j = 1:dimension($\boldsymbol{A}$) **do**
9. Nm ← *vpa*($\boldsymbol{A}$)
10. Nm(:,j) ← $\boldsymbol{B}$
11. I ← Compute determinant of Nm over D
12. $\boldsymbol{i}$(j) ← Perform inverse Laplace transform on I
13. **end**
14. return($\boldsymbol{i}$)

This paper has been accepted for publication in the AEE journal. This is the version, which has not been fully edited and content may change prior to final publication.
Citation information: DOI 10.24425/aee.2026.158258

To obtain the closed-form solution of Eq. (32), Algorithm 1 shows that the required input data are the model (corresponding to the particular cases presented as examples, with model structures 1.0, 2.0, and 2.1), the $\boldsymbol{R}$ and $\boldsymbol{L}$ matrices associated with the selected model (with element values taken from Table 1), and the field voltage. Through the procedure described in Algorithm 1 (the numerical values of the elements of matrix $\boldsymbol{A}$ are represented and manipulated with variable precision, using symbolic arithmetic through the *vpa* function of the Symbolic Math Toolbox), all relevant frequencies and coefficients are directly determined according to the supplied data. This is achieved without any simplification, approximation, or omission during the calculation process.

For the model structure 2.1 of the SM described in Table 1, the closed-form solution of the three-phase short-circuit currents obtained from (32) is shown in (33).

$$\boldsymbol{I} = \begin{pmatrix} i_d \\ i_q \\ i_F \\ i_D \\ i_Q \end{pmatrix} = \begin{pmatrix} 66701\cos(\omega_1 t)e^{\alpha t} - 2277\sin(\omega_1 t)e^{\alpha t} - 41097e^{s_1 t} - 15412e^{s_2 t} - 394e^{s_3 t} - 9798 \\ 36149\cos(\omega_1 t)e^{\alpha t} + 109800\sin(\omega_1 t)e^{\alpha t} + 57e^{s_1 t} - 221e^{s_2 t} - 36000e^{s_3 t} + 15 \\ -67\cos(\omega_1 t)e^{\alpha t} - 409\sin(\omega_1 t)e^{\alpha t} + 2323e^{s_1 t} - 2245e^{s_2 t} - 11e^{s_3 t} + 600 \\ -64023\cos(\omega_1 t)e^{\alpha t} + 10407\sin(\omega_1 t)e^{\alpha t} + 3636e^{s_1 t} + 59789e^{s_2 t} + 598e^{s_3 t} \\ -77663\cos(\omega_1 t)e^{\alpha t} - 212774\sin(\omega_1 t)e^{\alpha t} + 17e^{s_1 t} - 525e^{s_2 t} + 77121e^{s_3 t} \end{pmatrix}. \quad (33)$$

If the current vector $\boldsymbol{I}$ given in (29), and shown in expanded form in (33) for the model structure 2.1, is replaced in (32) according to the form $d\boldsymbol{I}/dt + \boldsymbol{L}^{-1}\boldsymbol{R}\boldsymbol{I} + \boldsymbol{L}^{-1}\boldsymbol{V} = \boldsymbol{\epsilon}$, the epsilon value approaches zero which means that the identity in (32) holds, as shown in Fig. 5.

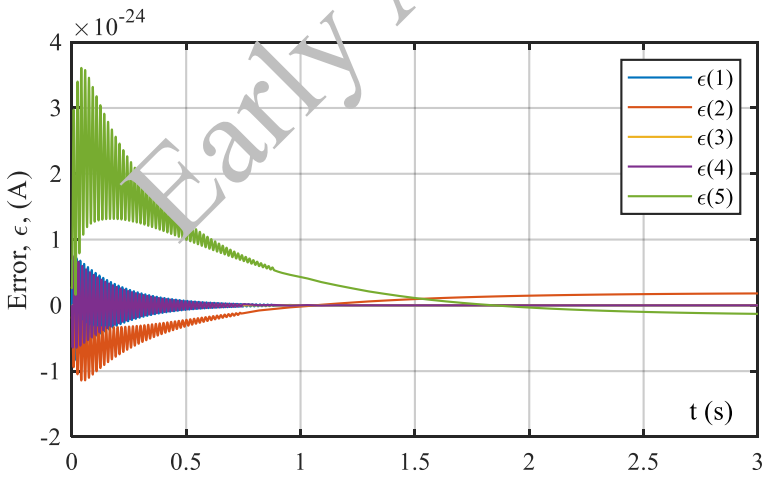

Fig. 5. Equivalent circuits for the model structure 2.0 of the SM in the 0*dq* domain

In (33), the influence of i_d on the other currents is captured in the first term of each current expression. Likewise, the influence of i_q on the other currents corresponds to the second term, and so on for i_F, i_D, and i_Q. The flux linkages among the windings of the SM are manifested through the mutual dependence of their currents. This interdependence is described by the short-circuit function through:

This paper has been accepted for publication in the AEE journal. This is the version, which has not been fully edited and content may change prior to final publication.
Citation information: DOI 10.24425/aee.2026.158258

– The coefficients k_{xy}, which represent the influence of the induced current "*y*" on the induced current "*x*," where *x* and *y* correspond to the *d*, *q*, *F*, *D*, and *Q* windings.
– The coefficients k_{zf}, which quantify the magnitude of the current under "quasi-steady-state" conditions when the fault is not cleared, where "*f*" denotes the forced value of the currents in the armature and field windings "z."
– The frequencies that determine the rate of variation and time duration of these currents - α and s_1 for the transient period, associated with the armature and field windings, respectively, and s_2 and s_3 for the sub-transient period, associated with the direct-axis and quadrature-axis damper windings, in that order.
– This dynamic interplay within the SM occurs simultaneously as the rotor rotates at the synchronous speed ω_1.

Recognizing this interdependence is one of the key advantages of expressing the currents in closed form. In column 4 of Table 3, for model structure 2.1, the values of frequencies ω_1, α, s_1, s_2, and s_3 are listed, along with the coefficients of currents i_d and i_q using notation consistent with the interdependence described above.

Table 3. Frequencies and coefficients of the armature current *i* in (35) for three model structures of the SM described in Table 1

Frequencies and coefficients	**Model structure**		
	1.0	**2.0**	**2.1**
ω_1	376.98	376.90	375.86
α	–1.6865	–2.1769	–4.9731
s_1	–1.6667	–1.5762	–1.5762
s_2	--	–69.241	–69.243
s_3	--	--	–140.75
K_{dd}	48 991	66 346	66 701
K_{dq}	45.891	–2 627.3	–2 276.8
K_{dF}	–39 193	–41 096	–41 096
K_{dD}	--	–15 452	–15 412
K_{dQ}	--	--	–394.43
K_{df}	–9 797.9	–9 797.9	–9 797.9
K_{qd}	–77.352	–103.96	36 149
K_{qq}	10 498	10 504	109 800
K_{qF}	61.882	64.887	57.006
K_{qD}	--	23.607	–221.60

This paper has been accepted for publication in the AEE journal. This is the version, which has not been fully edited and content may change prior to final publication.
Citation information: DOI 10.24425/aee.2026.158258

K_{qQ}	--	--	–36 000
K_{qf}	15.470	15.470	15.470

From the equation for currents in (5), the current vector $\boldsymbol{I}_{abc}$ is determined as given in (34), based on the currents i_d and i_q in (33).

$$\begin{pmatrix} i_a \\ i_b \\ i_c \end{pmatrix} = \sqrt{2/3} \begin{pmatrix} \cos(\theta) i_d + \sin(\theta) i_q \\ \cos(\theta - 120°) i_d + \sin(\theta - 120°) i_q \\ \cos(\theta + 120°) i_d + \sin(\theta + 120°) i_q \end{pmatrix}. \quad (34)$$

$\boldsymbol{I}_{abc}$ can also be obtained from (31) and is equivalent to (34) obtained from (5). From the $\boldsymbol{I}_{abc}$ vector in (34), the three-phase short-circuit current in the armature of the SM, for model structure 2.1, takes the form given in (35).

$$i = \begin{bmatrix} k\cos(\theta_i)(K_{dd}\cos(\omega_1 t)e^{\alpha t} + K_{dq}\sin(\omega_1 t)e^{\alpha t} + K_{dF}e^{s_1 t} + K_{dD}e^{s_2 t} + K_{dQ}e^{s_3 t} + K_{df}) \\ + k\sin(\theta_i)(K_{qd}\cos(\omega_1 t)e^{\alpha t} + K_{qq}\sin(\omega_1 t)e^{\alpha t} + K_{qF}e^{s_1 t} + K_{qD}e^{s_2 t} + K_{qQ}e^{s_3 t} + K_{qf}) \end{bmatrix}. \quad (35)$$

In (35) $k = \sqrt{2/3}$; if $i = i_a$, then according to (1), $\theta_i = \theta_a = \omega_1 t + 90°$ with $\delta = 0°$. The results for frequencies and coefficients in (35), listed in Table 3 (model 2.1), are independent of the value of δ.

The currents i_b e i_c have the same frequencies and coefficients as i_a, only the phase shift of 120°; thus, $\theta_b = \theta_a - 120°$ and $\theta_c = \theta_a + 120°$. The field current is given by (36), and the values of its coefficients are listed in Table 4 (see model 2.1).

$$i_F = K_{Fd}\cos(\omega_1 t)e^{\alpha t} + K_{Fq}\sin(\omega_1 t)e^{\alpha t} + K_{FF}e^{s_1 t} + K_{FD}e^{s_2 t} + K_{FQ}e^{s_3 t} + K_{Ff}. \quad (36)$$

Table 4. Coefficients of the field current i_F in (36) for three model structures of the SM described in Table 1

Coefficients	**Model Structure**		
	1.0	**2.0**	**2.1**
K_{Fd}	–2 400.1	–71.275	–66.844
K_{Fq}	–0.1260	–404.31	–408.75
K_{FF}	2 400.1	2 322.7	2 322.7
K_{FD}	--	–2 251.4	–2 245.3
K_{FQ}	--	--	–10.596
K_{Ff}	600	600	600

The estimated parameter values for the model structure 2.1 of the SM listed in Table 1 are also applied to structures 1.0 and 2.0 to determine the corresponding values of frequencies and

This paper has been accepted for publication in the AEE journal. This is the version, which has not been fully edited and content may change prior to final publication.
Citation information: DOI 10.24425/aee.2026.158258

coefficients. Although it is not accurate to apply parameter values to model structures different from the ones they were estimated for, this is done for comparative purposes. The values of frequencies and coefficients of the armature current i given by (35) and the coefficients of the field current i_F given by (36) for model structures 1.0 and 2.0 are also listed in Tables 3 and 4, respectively.

In Fig. 6, the envelopes (solid lines) of the three-phase short-circuit current of the SM and its asymmetry (dashed lines) are shown in the armature (phases a, b, and c) and in the field winding i_F, according to model structures 1.0, 2.0, and 2.1, and based on the parameter values listed in Table 1.

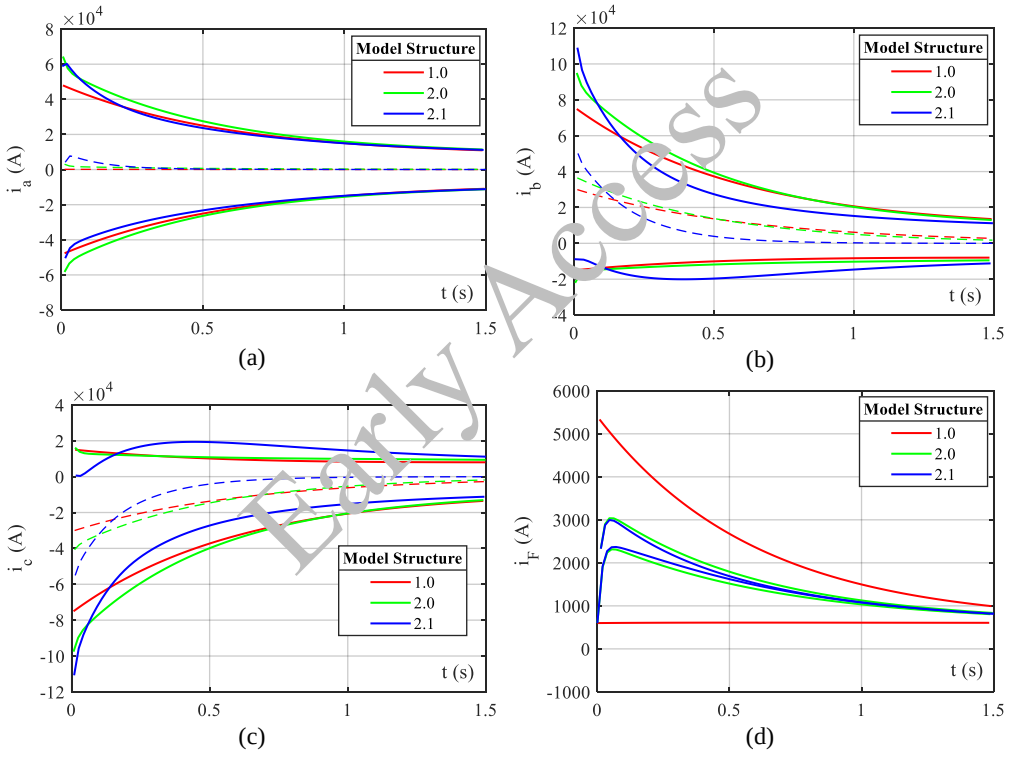

Fig. 6. Envelopes of the three-phase short circuit current of the SM described in Table 1, according to model structures 1.0, 2.0, and 2.1: (a) i_a; (b) i_b; (c) i_c; (d) i_F

3.1. Synchronic frequency variation

The value of the synchronous frequency $\omega_s = 120\,\pi$, at which the SM is operating in steady state, changes to the value ω_1 during the transient condition of three-phase short-circuit, as observed in Table 3, decreasing by up to 0.3% of ω_s for model structure 2.1. However, during the first four cycles, the frequency of the synchronous component of the fault current changes from 410 rad/sec until it stabilizes at ω_1.

This paper has been accepted for publication in the AEE journal. This is the version, which has not been fully edited and content may change prior to final publication.
Citation information: DOI 10.24425/aee.2026.158258

Such decrease in frequency is anticipated when considering the change in operating condition of the machine, transitioning from the no-load condition to suddenly receiving maximum load, namely, the three-phase short-circuit condition. The change in energy in the windings of the machine due to its change in operation is what affects its frequency change.

The variation in frequency, resulting from the change in energy in the windings of the SM, can be evaluated if the complete model (i.e., the estimated value of the parameters R_a and L of its windings corresponding to its model structure) is brought into the three-phase short-circuit condition, allowing the hypothetical variation of each parameter one at a time.

In Fig. 7, the mentioned evaluation can be observed for model structure 2.1 of the SM described in Table 1, when varying the parameters L and R_a of the windings. For instance, if all parameters of the machine (see Table 1) remain constant except for those related to the self-inductances, as indicated by the percentage in Fig. 7(a), it shows how increasing the values of L_q and L_Q has a greater influence than the other inductances in bringing the frequency of the SM closer to the nominal steady-state frequency under three-phase short-circuit condition.

Considering the previous result, namely, that the greatest sensitivity to frequency increase occurs if the value of L_q could be increased, Fig. 7(b) presents the variation of this parameter along with R_a, in the percentage indicated there. In Fig. 7(b) it is observed that only if the value of R_a approaches zero ohms and/or the value of L_q is increased, the frequency would tend towards its nominal value.

As mentioned, the variation of the parameters is hypothetical because the SM is already built. However, the analysis presented here could be considered in future design stages for its construction.

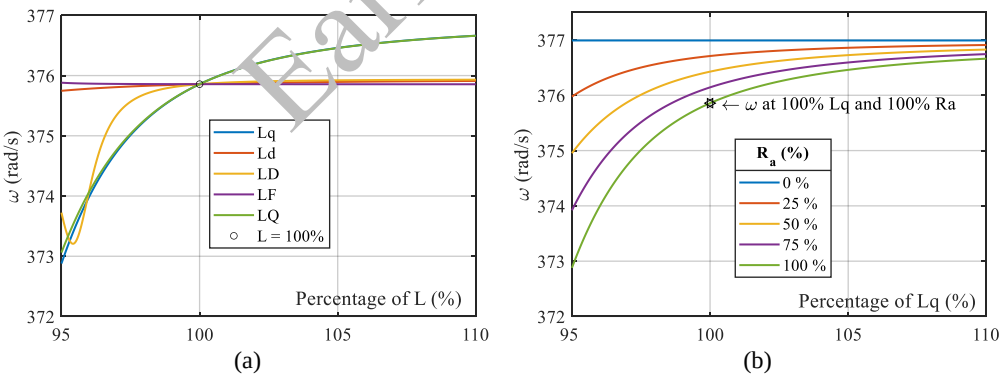

Fig. 7. Variation of ω in the SM described in Table 1, with model structure 2.1, due to change from steady state to three-phase short circuit: (a) varying one L at the time; (b) varying L_q and R_a

4. Components of the three-phase short-circuit current

This paper has been accepted for publication in the AEE journal. This is the version, which has not been fully edited and content may change prior to final publication.
Citation information: DOI 10.24425/aee.2026.158258

The composition of the three-phase fault current in the SM [14, 17] given in (35) allows the identification of its behavior in terms of its analytical form and its amplitude or intensity. This current is expressed by components as follows: the fundamental frequency or *ac component*, which is symmetric with respect to the time axis; the *dc component*, which gives it asymmetric shape; and the *second harmonic component* (double frequency).

The current given by Eq. (35), written for each of the phases *a*, *b*, and *c*, is reformulated as the sum of its *ac*, *dc*, and *double-frequency components* after applying algebraic and trigonometric manipulations (without any omission or simplification during the process), considering the angle δ. The resulting expressions are presented in Eqs. (37) to (45).

$$i_{a(ac)} = k\begin{bmatrix}(K_{df} + K_{dF}e^{s_1 t} + K_{dD}e^{s_2 t} + K_{dQ}e^{s_3 t})\cos(\theta_a + \delta°)\\ +(K_{qf} + K_{qF}e^{s_1 t} + K_{qD}e^{s_2 t} + K_{qQ}e^{s_3 t})\sin(\theta_a + \delta°)\end{bmatrix}, \tag{37}$$

$$i_{a(dc)} = -\frac{k}{2}\left[(K_{qq} + K_{dd})\sin\delta° - (K_{qd} - K_{dq})\cos\delta°\right]e^{\alpha t}, \tag{38}$$

$$i_{a(2\omega)} = \frac{k}{2}\begin{bmatrix}\sqrt{K_{dd}^2 + K_{dq}^2}\sin\left((2\theta_a + \delta°) - \tan^{-1}\frac{K_{dq}}{K_{dd}}\right)\\ -\sqrt{K_{qd}^2 + K_{qq}^2}\cos\left((2\theta_a + \delta°) - \tan^{-1}\frac{K_{qq}}{K_{qd}}\right)\end{bmatrix}e^{\alpha t}, \tag{39}$$

$$i_{b(ac)} = k\begin{bmatrix}(K_{df} + K_{dF}e^{s_1 t} + K_{dD}e^{s_2 t} + K_{dQ}e^{s_3 t})\cos(\theta_b + \delta°)\\ +(K_{qf} + K_{qF}e^{s_1 t} + K_{qD}e^{s_2 t} + K_{qQ}e^{s_3 t})\sin(\theta_b + \delta°)\end{bmatrix}, \tag{40}$$

$$i_{b(dc)} = \frac{k}{4}\begin{Bmatrix}\left[\sqrt{3}(K_{dd} + K_{qq}) + K_{dq} - K_{qd}\right]\cos\delta°\\ +\left[\sqrt{3}(K_{qd} - K_{dq}) + K_{dd} + K_{qq}\right]\sin\delta°\end{Bmatrix}e^{\alpha t}, \tag{41}$$

$$i_{b(2\omega)} = \frac{k}{2}\begin{bmatrix}\sqrt{K_{dd}^2 + K_{dq}^2}\cos\left((2\theta_b + \delta°) - \tan^{-1}\frac{\sqrt{3}K_{dq} - K_{dd}}{K_{dq} + \sqrt{3}K_{dd}}\right)\\ +\sqrt{K_{qd}^2 + K_{qq}^2}\cos\left((2\theta_b + \delta°) - \tan^{-1}\frac{\sqrt{3}K_{qd} + K_{qq}}{K_{qd} - \sqrt{3}K_{qq}}\right)\end{bmatrix}e^{\alpha t}, \tag{42}$$

$$i_{c(ac)} = k\begin{bmatrix}(K_{df} + K_{dF}e^{s_1 t} + K_{dD}e^{s_2 t} + K_{dQ}e^{s_3 t})\cos(\theta_c + \delta°)\\ +(K_{qf} + K_{qF}e^{s_1 t} + K_{qD}e^{s_2 t} + K_{qQ}e^{s_3 t})\sin(\theta_c + \delta°)\end{bmatrix}, \tag{43}$$

$$i_{c(dc)} = \frac{k}{4}\begin{Bmatrix}\left[K_{dq} - K_{qd} - \sqrt{3}(K_{dd} + K_{qq})\right]\cos\delta°\\ +\left[\sqrt{3}(K_{dq} - K_{qd}) + K_{dd} + K_{qq}\right]\sin\delta°\end{Bmatrix}e^{\alpha t}, \tag{44}$$

$$i_{c(2\omega)} = \frac{k}{2}\begin{bmatrix}\sqrt{K_{dd}^2 + K_{dq}^2}\cos\left((2\theta_c + \delta°) + \tan^{-1}\frac{\sqrt{3}K_{dq} + K_{dd}}{K_{dq} - \sqrt{3}K_{dd}}\right)\\ +\sqrt{K_{qd}^2 + K_{qq}^2}\cos\left((2\theta_c + \delta°) + \tan^{-1}\frac{\sqrt{3}K_{qd} - K_{qq}}{K_{qd} + \sqrt{3}K_{qq}}\right)\end{bmatrix}e^{\alpha t}. \tag{45}$$

This paper has been accepted for publication in the AEE journal. This is the version, which has not been fully edited and content may change prior to final publication.
Citation information: DOI 10.24425/aee.2026.158258

Figure 8 shows the behaviors of the three-phase short-circuit current components (the envelopes are shown for *synchronous* and *double frequency components*) of phase *a*, with $\delta = 0°$, according to model structures 1.0, 2.0, and 2.1.

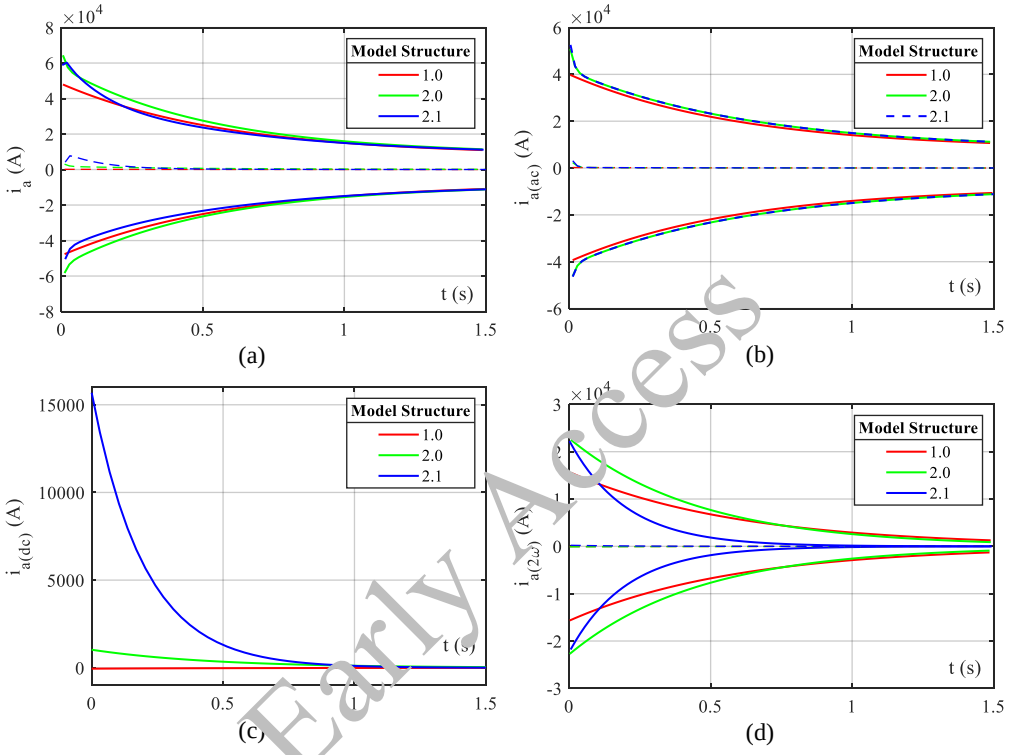

Fig. 8. Three-phase short-circuit current components for phase *a* with $\delta = 0°$ of the SM described in Table 1, according to model structures: (a) i_a; (b) $i_{a(ac)}$; (c) $i_{a(dc)}$; (d) $i_{a(2\omega)}$

4.1. Impact of the variation of δ on the current

For the SM under load, the angles δ and φ ($= \theta_v - \theta_i$) of the load power factor may not be zero, thus the magnitude of fault currents can vary. From circuit theory, assuming $\theta_v = 0°$ for phase *a*, it is possible to consider the load power factor with the angle θi of its current; that is, conveniently superimposing the angle φ of the power factor onto $\theta_a = \omega t + 90°$. Thus, the angles δ and φ can be superimposed onto θ_i to observe how the magnitude of the short-circuit current changes in each of its phases when considering the SM when loaded at the fault.

The effect of varying the angle δ on the magnitude of the three-phase fault current can be observed by plotting Eqs. (37) to (45). In these plots, the *ac* and *double frequency components* appear shifted to the left by the angle in degrees of δ, without modifying their shape or the magnitude of their envelope. However, the *dc component* of each phase (evaluated at $t = 0$) varies in magnitude, as shown in Fig. 9 for model structures 1.0, 2.0, and 2.1. This variation does impact

This paper has been accepted for publication in the AEE journal. This is the version, which has not been fully edited and content may change prior to final publication.
Citation information: DOI 10.24425/aee.2026.158258

the magnitude of the short-circuit current, and it's worth noting that the highest magnitude falls on phase *b*, regardless of the model structure being referenced, whose maximum coincides with the intersection of the curves of that component between phases *a* and *c*.

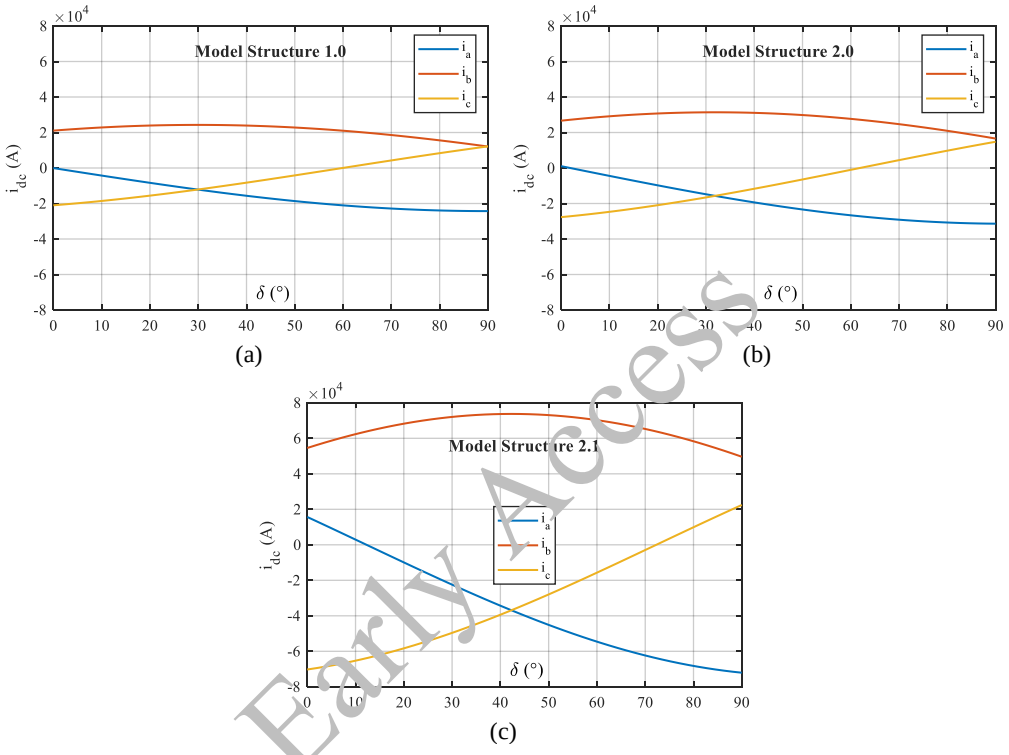

Fig. 9. Variation of the *dc* component at $t = 0$ of the three-phase short-circuit current for $0° \leq \delta \leq 90°$, according to model structures: (a) 1.0; (b) 2.0; (c) 2.1

Now, focusing on the *dc component* of phase *b* current for model 2.1, Fig. 10 presents the hypothetical scenario of varying the values of the machine's inductances, one at the time (while the others remain at their nominal values.) For this scenario, Fig. 10(a) displays the maximum *dc* current value, while Fig. 10(b) shows the angle δ at which this maximum current occurs. Note that increasing the self-inductance of any of the coils results in a maximum current of lower magnitude.

This paper has been accepted for publication in the AEE journal. This is the version, which has not been fully edited and content may change prior to final publication.
Citation information: DOI 10.24425/aee.2026.158258

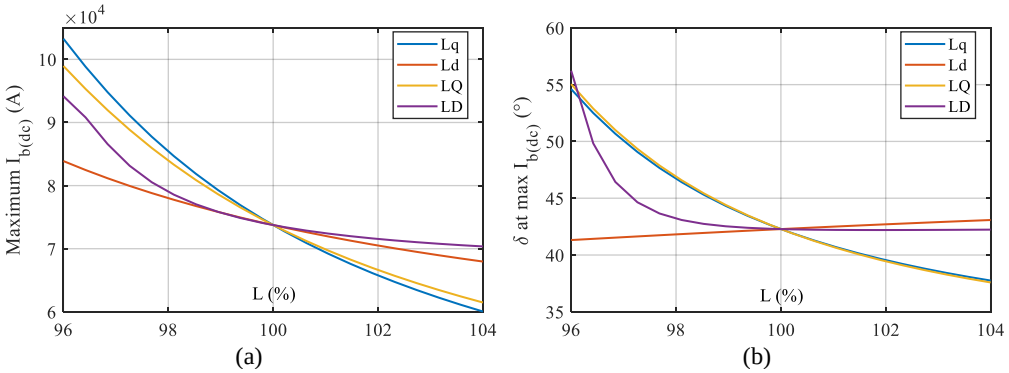

Fig. 10. Variation of the *dc component* of i_b for model structure 2.1 as a function of changes in the inductances: (a) maximum *dc* current value; (b) angle δ at which this maximum current occurs

5. Closed-form and discrete solutions comparison

This section establishes a comparison of three-phase fault calculation between closed and discrete forms (numerical integration using the ode45 algorithm.) According to the three-phase short-circuit calculation results for model structure 2.1 of the SM, and considering the closed-form results as exact, those obtained in discrete form are compared in terms of magnitude and phase for two relative tolerances, as shown in Fig. 11.

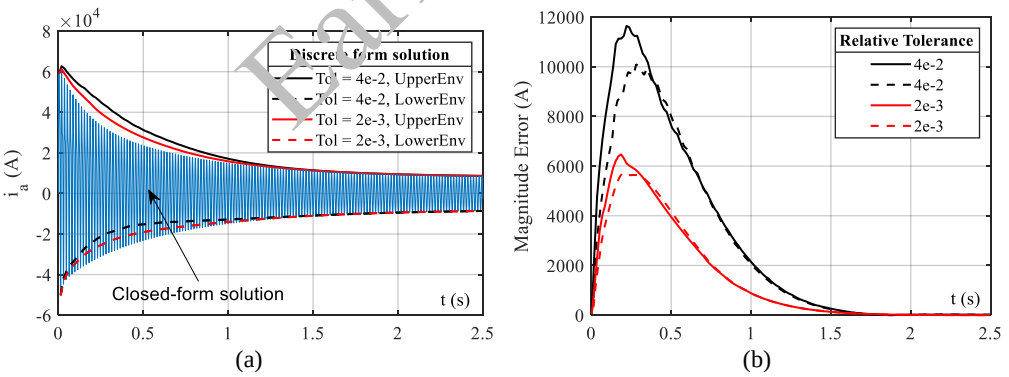

This paper has been accepted for publication in the AEE journal. This is the version, which has not been fully edited and content may change prior to final publication.
Citation information: DOI 10.24425/aee.2026.158258

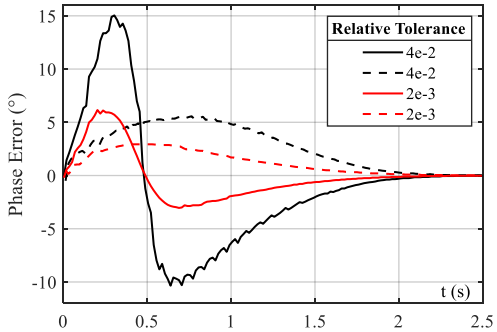

(c)

Fig. 11.Comparison of the discrete forms (2 relative tolerances) and continuous form of the three-phase short-circuit current i_a for model structure 2.1: (a) significant mismatch at the start of the transient period; (b) magnitude error; (c) phase error

As observed in Fig. 11(a), with lower relative error tolerance, the solution in discrete form approximates more closely, in both magnitude and phase, to the closed form, thus considered exact. Note that the phase error is also corrected in the calculation of the discrete form, from which it can be inferred that in both solution forms the frequency during the fault remains the same, i.e., ω_1.

The magnitude error (see Fig. 11(b)) results from the comparison between maximum points (solid lines) or minimum points (dashed lines) of the closed form with the corresponding ones for each relative tolerance. These maximum (or minimum) points of the closed form do not coincide in time with their corresponding ones found in discrete form, resulting in a phase error shown in Fig. 11(c).

The error in the discrete solution is decreased decreasing the relative tolerance, which would make the curve fit closer to the one obtained using closed-form solution, at the expense of requiring more computational effort (a higher number of iterations) and computation time. This can be observed in Fig. 12 where the two solutions are compared in terms of computation time and maximum error in short-circuit current amplitude, considering the variation of relative tolerance in the discrete solution. In Fig. 12(a), it is observed that computation times are always shorter in the closed-form solution, while they increase in the discrete solution with lower relative tolerance. It is expected that a discrete solution could require less computation time than the closed one if a higher relative tolerance were allowed. However, the calculation results would exceed by 10^3 the error order of the solution compared to the closed form, as shown in Fig. 12(b).

This paper has been accepted for publication in the AEE journal. This is the version, which has not been fully edited and content may change prior to final publication.
Citation information: DOI 10.24425/aee.2026.158258

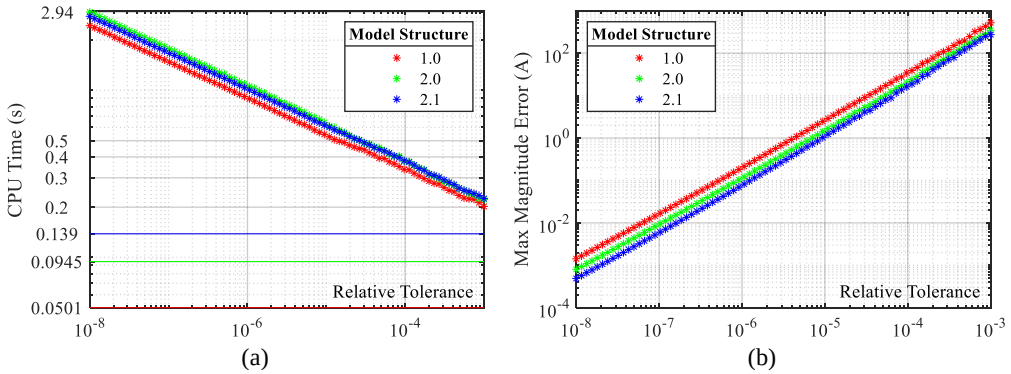

Fig. 12. Comparison of closed and discrete solutions of current i_a for the three model structures of the SM described in Table 1: (a) CPU time; (b) maximum magnitude error

6. Conclusions

It is possible to derive a closed-form solution for the generator under a three-phase short-circuit condition. The deterministic "short-circuit function" of the synchronous machine in the transient state can be obtained—regardless of the level of modeling complexity—following the different model structures described in IEEE Std 1110-2002. This solution provides a mathematically coherent description of the simultaneous and interrelated transient behaviors among the machine windings, enabling analytical observation of their *synchronous*, *dc*, and *double-frequency* components for each phase.

Model structure 2.1 of IEEE Std 1110-2002 is considered the basic and reasonably detailed level of complexity for representing the synchronous machine with its six windings (phases *a*, *b*, and *c*; field winding *F*; and damper windings *D* and *Q*). The results for the magnitude of the three-phase short-circuit current obtained with the 2.1 model show that this current more accurately reflects the machine's actual behavior compared with models 1.0 and 2.0. This underscores the importance of including quadrature-axis generator data derived from the SSFR frequency-response test.

The closed-form solution provides broad, complete, and precise information on the synchronous machine (SM) in the transient state. In this study, the closed-form solution enabled the following contributions:

– **Interdependent behavior of the windings.** The flux linkages among the SM windings give rise to the mutual dependence of their currents, which the short-circuit function characterizes through the coefficients k_{xy} (influence of induced current "*y*" on induced current "*x*," where *x* and *y* correspond to the *d*, *q*, *F*, *D*, and *Q* windings); the coefficients k_{zf} (which quantify the magnitude of the current under "quasi-steady-state" conditions, where "*f*" denotes the forced value of the armature and field currents "*z*"); and the characteristic frequencies of these currents (transient frequencies α and s_1 for the armature

This paper has been accepted for publication in the AEE journal. This is the version, which has not been fully edited and content may change prior to final publication.
Citation information: DOI 10.24425/aee.2026.158258

and field windings, respectively, and sub-transient frequencies s_2 and s_3 for the direct- and quadrature-axis damper windings), all while the rotor rotates at the synchronous speed ω_1.

– **Variation in synchronous frequency.** The synchronous frequency ω_s, at which the SM operates in steady state, changes under the transient three-phase short-circuit condition to the value ω_1. The energy redistribution among the windings during this change of operating condition drives the shift in frequency. If, during machine design, the armature resistance R_a is made to approach zero and/or the quadrature-axis inductance L_q is increased, the short-circuit frequency ω_1 approaches the steady-state nominal value ω_s.

– **Impact of δ variation on current.** The effect of variations in the angle δ on the three-phase fault current is analytically evident when the short-circuit function is expressed through its *ac*, *dc*, and *double-frequency* components. While the *ac* and *double-frequency* components shift horizontally by the angle change in δ, the *dc* component (evaluated at $t = 0$) changes in magnitude, thus affecting the short-circuit current. The largest magnitude variation occurs in phase *b*, regardless of the model structure used, and its maximum coincides with the intersection of the curves for that component between phases *a* and *c*.

Moreover, the closed-form solution offers advantages over numerical integration techniques. For example, in terms of efficiency, the closed-form solution for model structure 2.1 is twenty times faster than its discrete counterpart. Computationally, it is executed in a single operation, as opposed to the point-by-point temporal approach required by the discretized solution. Furthermore, with respect to accuracy, variations in both the magnitude and phase of the fault current during the transient period are observed.

The closed-form solution provides a fully adequate formal analytical description of the synchronous machine in its dynamic transient state. In future studies, additional insight into the deterministic short-circuit function may be obtained by considering, for example, the rotor mass inertia or the ground-fault impedance. It is also of interest to establish similarities between the closed-form solution and the empirical short-circuit function derived from estimating the "characteristic quantities" (time constants and reactances) using SSC test data from the unloaded SM. This information—together with the use of the closed-form solution in stability studies, given its advantages over simulation-based methods—supports the advancement of the electric power industry in the field of power systems.

References

[1] Boboń A., Berhausen S., *Determination of high power synchronous generator subtransient reactances based on the waveforms for a steady state two-phase short-circuit*, Applied Mathematics and Computation, vol. 319, pp. 538–550 (2018), DOI: 10.1016/j.amc.2017.06.003.

[2] Wang J., Zhou L., Yang R., Xiao Y., *Finite Element Computation of Transient Parameters of a Salient-Pole Synchronous Machine*, Energies, vol. 10, no. 7, pp. 1–18 (2017), DOI: 10.3390/en10071015.

[3] Hegner H.J., Wasynczuk 0., Pekarek S.D., *An Efficient and Accurate Model for the Simulation and Analysis of Synchronous Machine/Converter Systems*, IEEE Transactions on Energy Conversion, vol. 13, no. 1, pp. 42–48 (1998), DOI: 10.1109/60.658202.

This paper has been accepted for publication in the AEE journal. This is the version, which has not been fully edited and content may change prior to final publication.
Citation information: DOI 10.24425/aee.2026.158258

[4] Jatskevich J., Wang L., *A Voltage-Behind-Reactance Synchronous Machine Model for the EMTP-Type Solution*, IEEE Transactions on Power Systems, vol. 21, no. 4, pp. 1539–1549 (2006), DOI: 10.1109/TPWRS.2006.883670.
[5] Lupșa-Tătaru L., *Comparative Simulation Study on Synchronous Generators Sudden Short Circuits*, Modelling and Simulation in Engineering, vol. 2009, no. 867150, pp. 1–11 (2009), DOI: 10.1155/2009/867150.
[6] Dommel H.W., Jatskevich J., Wang L., *Re-examination of Synchronous Machine Modeling Techniques for Electromagnetic Transient Simulations*, IEEE Transactions on Power Systems, vol. 22, no. 3, pp. 1221–1230 (2007), DOI: 10.1109/TPWRS.2007.901308.
[7] Neamt L., Chiver O., Matei O., *Comparative study on sudden short-circuit currents of a synchronous generator*, 2015 IEEE 15th International Conference on Environment and Electrical Engineering (EEEIC), Rome, Italy, pp. 1–6 (2015), DOI: 10.1109/EEEIC.2015.7165426.
[8] Hackbart M., *Novel approach to calculate electrical currents in stator-, field- and damper-windings at three-phase sudden short-circuit for large synchronous generators*, e & i Elektrotechnik und Informationstechnik, vol. 133, no. 2, pp. 112–120 (2016), DOI: 10.1007/s00502-016-0389-7.
[9] Jäger C., Grinbaum I., Smajic J., *Dynamic Short-Circuit Analysis of Synchronous Machines*, IEEE Transactions on Magnetics, vol. 53, no. 6, pp. 1–4 (2017), DOI: 10.1109/TMAG.2017.2661580.
[10] Hassan M.A., *Dynamic Behavior Analysis of Synchronous Generator Using MATLAB/SIMULINK*, 2015 International Conference on Computing, Control, Networking, Electronics and Embedded Systems Engineering (ICCNEEE), Khartoum, Sudan, pp. 143–148 (2015), DOI: 10.1109/ICCNEEE.2015.7381445.
[11] IEEE Power and Energy Society, *Guide for Test Procedures for Synchronous Machines Including Acceptance and Performance Testing and Parameter Determination for Dynamic Analysis*, IEEE Std 115™ (2019).
[12] IEEE Power and Energy Society, *IEEE Guide for Synchronous Generator Modeling Practices and Applications in Power System Stability Analyses*, IEEE Std 1110™ (2002).
[13] Belqorchi A., Kamwa I., Mahseredjian J., Karaagac U., *Standstill Frequency Response Test and Validation of a Large Hydrogenerator*, IEEE Transactions on Power Systems, vol. 34, no. 3, pp. 2261−2269 (2019), DOI: 10.1109/TPWRS.2018.2889510.
[14] Saadat H., *Synchronous Machine Transient Analysis*, *Power System Analysis*, McGraw-Hill International Editions, WCB (1999).
[15] Padiyar K.R., *Modeling of Synchronous Machine*, *Power System Dynamics, Stability and Control*, 2nd ed., AP: BS Publications (2008).
[16] Anderson P.M., *Sequence Impedance of Machines*, *Analysis of Faulted Power Systems*; IEEE PRESS Power Systems Engineering Series; John Wiley & Sons Inc. (1995).
[17] Guevara G.A., Rairán J.D., *Advancements in Three-Phase Short-Circuit Fault Computation for Power System Generators: A Comprehensive Review*, Revista Facultad de Ingeniería, vol. 33, no. 67 (2024), DOI: 10.19053/uptc.01211129.v33.n67.2024.15945.
[18] Kuhn B.T., Aliprantis D.C., Sudhoff S.D., *A Synchronous Machine Model With Saturation and Arbitrary Rotor Network Representation*, IEEE Transactions on Energy Conversion, vol. 20, no. 3, pp. 584–594 (2005), DOI: 10.1109/TEC.2005.845455.
[19] Capolino G.A., Henao H., Rehaoulia H., *Modeling of Synchronous Machines with Magnetic Saturation*, Electric Power Systems Research, vol. 77, pp. 652–659 (2006), DOI: 10.1016/j.epsr.2006.06.003.
[20] Saidi A.S., *A Nonlinear Saturation Model of Synchronous Machines with Account Cross Saturation*, International Journal of Advanced and Applied Sciences, vol. 6, no. 9, pp. 20–24 (2019), DOI: 10.21833/ijaas.2019.09.003.
[21] Park R.H., *Two Reaction Theory of Synchronous Machines, Generalized Method of Analysis-Part I*, Transactions of the American Institute of Electrical Engineers, vol. 48, no. 3, pp. 716–727 (1929), DOI: 10.1109/T-AIEE.1929.5055275.

This paper has been accepted for publication in the AEE journal. This is the version, which has not been fully edited and content may change prior to final publication.
Citation information: DOI 10.24425/aee.2026.158258

[22] Park R.H., *Two Reaction Theory of Synchronous Machines – II*, Transactions of the American Institute of Electrical Engineers, vol. 52, no. 2, pp. 352–354 (1933), DOI: 10.1109/T-AIEE.1933.5056309.
[23] Lipo T.A., *Transient Analysis of Synchronous Machines*, *Analysis of Synchronous Machines*, 2nd ed., Taylor & Francis Group, LLC; CRC Press (2012).
[24] Sianipar G., *Closed Form Solution of Synchronous Machine Short Circuit Transients*, ITB Journal of Engineering Science, vol. 42, no. 1, pp. 91–102 (2010), DOI: 10.5614/itbj.eng.sci.2010.42.1.7.
[25] Kundur P., *Sychronous Machine Theory and Modelling*, *Power System Stability and Control*, EPRI Eds.; McGraw-Hill, Inc. (1994).
[26] Adkins B., Harley R.G., *The General Theory of Alternating Current Machines: Application to Practical Problems*, Chapman and Hall (1975).